Journal of Engineering, Project, and Production Management
2026, 16(5), 2025-368

A Hybrid ADMM-IPM Framework for Secure and Efficient Joint Clearing of Electricity and Ancillary Service Markets

Xingyou Zhang[1], Yuanlong Liu[2], Qiang Ma[3], Shan Li[4], Congcong Liu[5], and Jing Yao[6]
[1] Senior Engineer, State Grid Shandong Electric Power Company, Jinan, 250013, China, E-mail: zhxyou_sd@163.com
[2] Director, State Grid Shandong Electric Power Research Institute, Jinan, 250003, China, E-mail: Liuyuanlong@sd.sgcc.com.cm
[3] Senior Engineer, State Grid Shandong Electric Power Research Institute, Jinan, 250003, China, E-mail: Maqiang@sd.sgcc.com.cn
[4] Engineer, State Grid Shandong Electric Power Research Institute, Jinan, 250003, China, E-mail: lis0903@163.com
[5] Engineer, State Grid Shandong Electric Power Company, Jinan, 250013, China, E-mail: ccliusdu@126.com
[6] Engineer, Beijing TsIntergy Technology Co., Ltd, Beijing, 102200, China, E-mail: yaojing_91@163.com (corresponding author).

Project Management
Received December 30, 2025; revised March 1, 2026; accepted April 7, 2026
Available online June 17, 2026

Abstract: This study addresses the low computational efficiency and safety verification challenges in joint clearing of electricity and ancillary service markets (e.g., frequency regulation and reserve) caused by deep market coupling and multi-participant participation. A hybrid solution framework combining the Alternating Direction Method of Multipliers (ADMM) and Interior Point Method (IPM) is proposed to efficiently solve high-dimensional non-convex optimization problems through a hierarchical "external decomposition internal refinement" strategy. At the outer coordination level, ADMM exploits problem separability to enable distributed decomposition across multiple trading products and cross-regional markets, significantly reducing problem scale via parallel computation. The Interior Point Method (IPM) is employed to accurately solve nonlinear Optimal Power Flow (OPF) sub-problems with Alternating Current (AC) power flow constraints, ensuring high solution precision and feasibility. Furthermore, safety constraint checking and feedback correction are embedded to form a closed-loop "optimization-verification-correction" mechanism, enabling full-timescale power flow security regulation. Experiments show that this method, under conditions of high volatility (±15% load variation) and high renewable energy penetration (50%), can complete market clearing in only 46 iterations (average 150 seconds), with a total electricity purchase cost of US$5.6 million. Furthermore, it achieves a safe reschedule within 9.3 seconds after a sudden fault, significantly outperforming existing methods. This method significantly improves the clearing efficiency and reliability of high-proportion renewable energy power markets, providing a practical optimization tool for actual dispatch operations.

Keywords: Electricity and ancillary services, alternating direction method of multipliers, interior-point method, multiple subjects, hybrid solution.

Copyright © Journal of Engineering, Project, and Production Management (EPPM-Journal).
DOI 10.32738/JEPPM-2025-368

1. Introduction

1.1. Research Background

This coupling of electric energy to ancillary services, including frequency regulation and reserves, continues to grow in new power systems. Market clearing should be able to address at the same time the two complementary requirements of multi-dimensional resource coordination and grid security (Zahedmanesh et al., 2021; Scolaro and Kittner, 2022). The large-scale participation of entities has led to full-bid interleaving of bidding behavior and physical constraints, making classical, separated dispatch models difficult to adapt to complex interactive requirements (Hossain et al., 2023). As the core means to achieve optimal value allocation, joint clearing urgently needs to overcome the technical challenges of collaborative modeling for economic efficiency and safety (Levin et al., 2023; Thukral, 2021; Catalan et al., 2023). Its evolution has significant impacts not only on market efficiency and fairness, but also directly on the system's dynamic balancing capability

in highly uncertain environments (Xing et al., 2025; Li et al., 2025). It has become crucially pivotal in the development of the contemporary power market.

Current joint clearing algorithms suffer from substantial bottlenecks when faced with high-dimensional, non-convex optimization problems. When electricity and several ancillary services are co-optimized in an aggregated model, the synergistic effect of coupling the objective function to the constraint set is significantly increased, leading to slow convergence, or even stalling in the solution procedure (Yang et al., 2021; Jiang et al., 2022). In particular, because of new types of participating units, such as Distributed Energy Resources (DERs), energy storage, and load aggregators, the dimension of variables increases exponentially, and the classical centralized solution approaches cannot find a complete set of feasible solutions within a given timeframe (Lu et al., 2022; Zou et al., 2022). Certain protocols aim at alleviating the computational load by coarsening the network model or relaxing the safety constraints, but the obtained solutions may violate the real feasible operating boundaries, which renders the physical feasibility of dispatch instructions questionable (Jiang et al., 2021; Liu et al., 2024). Other methods are based on predefined scenario reduction or heuristic iteration. Although these approaches can enhance the convergence speed to a certain extent, they are not guaranteed to achieve global optimality (Zhang et al., 2021; He et al., 2022). In addition, information barriers and data heterogeneity for cross-regional trade make the problem harder to coordinate, and a unique central node that gathers all the information of the network may result in an extreme double bottleneck of communication and computation (Zou 2024; Chen et al., 2022). More importantly, safety verification is usually performed as an additional post-clearing procedure in several markets, which can prevent the incorporation of feedback results into the clearing process. This prompts some apparently economical schemes to fail often when they are rechecked by power flow, which requires the price to be adjusted or the iteration to continue for many times, causing an extremely time-consuming and unstable procedure (Wu et al., 2022; Chen et al., 2021). This kind of phenomenon implies that at least the existing technical means are far from optimal in view of the trade-off among model expressiveness, algorithm robustness, and engineering applicability.

1.2. Limitations of Existing Methods

Early work often cleared electricity and ancillary services in sequence, taking a stepwise approach to optimization to ameliorate solution pressures associated with high-dimensional coupling (Dong et al., 2022; Ma et al., 2024). Scholars have proposed a unified clearing framework to enhance the efficiency of resource allocation by bringing different services under a single objective function and capturing differences in marginal costs through Lagrange multipliers (He et al., 2021; Tsaousoglou et al., 2021). For linearized mixed integer programming problems, Bender's decomposition has been widely used (Jacobson et al., 2024; Shelar et al., 2021). The former is suitable for small-scale systems, while the latter separates investment and operation decisions through a master-slave structure. Some work introduces stochastic optimization to address uncertainty, constructs stage models, and combines scenario-generation technology to minimize expected costs (Antoniadou-Plytaria et al., 2022; Vera et al., 2022). In terms of safety constraints, Direct Current (DC) power flow approximation has become the mainstream choice, simplifying the power transmission relationship and enabling large-scale systems to be solved within a reasonable time (Huang et al., 2022). However, such methods are generally based on strong assumptions, which include ignoring changes in voltage amplitude, reactive power effects, and nonlinear loss terms, thereby failing to guarantee Alternating Current (AC) feasibility. Although there have been attempts to improve the computational architecture using the ideas of decomposition and coordination (Wang et al., 2023), most of them remain at the theoretical level, with a crude design of the information interaction mechanism between sub-problems and a lack of quantitative evaluation of convergence and accuracy loss. Overall, existing results have made many compromises between model fidelity and computational efficiency, failing to provide a systematic solution that combines scalability, security, and practical accuracy.

In recent years, the Alternating Direction Method of Multipliers (ADMM) has attracted attention due to its good decomposability and distributed implementation potential. Some studies have applied it to the decentralized dispatching of regional power systems, achieved coordinated optimization of cross-regional interconnection line power, and verified the convergence performance of the algorithm in weak coupling scenarios (Xiao et al., 2024; Kiani et al., 2023). The Interior-Point Method (IPM) has been integrated into the optimal power flow calculation module due to its advantages in handling nonlinear constraints and large sparse matrices. It has demonstrated high numerical stability and convergence speed and is used for relay protection coordination (Alam et al., 2024). Some explorations have attempted to combine the two, first using ADMM to split the regional sub-problems, and then using IPM to solve the nonlinear optimal power flow in each sub-domain, which has preliminarily demonstrated the feasibility of the hybrid architecture (Costantini and Görges, 2021). In addition, some teams have embedded a safety-constraint verification link into the ADMM framework and enhanced the physical consistency of the clearing results by triggering a correction mechanism via residual monitoring (Gholami et al., 2023). However, most existing hybrid applications are limited to idealized test systems and do not fully consider realistic factors such as the diversity of quotation strategies, equipment action timing constraints, and multi-service response priorities in the real market. More importantly, the penalty parameter setting of ADMM lacks an adaptive mechanism, and fixed parameters are prone to oscillation or slow convergence. IPM does not specifically strengthen the thermal stability and transient stability boundaries in the sub-problem solving, and the safety check is still a passive verification rather than active guidance. In addition, the entire process does not establish a closed-loop feedback structure, and it is impossible to dynamically adjust the Lagrange multiplier or constraint boundary according to the verification deviation, which limits the robust performance of the algorithm under complex working conditions. Although there are preliminary explorations of combining ADMM with Interior-Point Method (IPM), these attempts mostly remain in the theoretical verification stage, and their safety check is still an independent post-process link that fails to form dynamic feedback. In addition, the model does not adequately characterize the differentiated response characteristics of multiple subjects, resulting in substantial challenges to the applicability and safety of the method in the real market environment. Therefore, there is an urgent need to build a

new hybrid solution system that integrates the decomposition-coordination architecture with a high-precision local solver and has a built-in safety closed-loop mechanism.

1.3. Research Contributions

In response to the above core challenges, this paper proposes a technical approach to joint clearing of electricity and ancillary services across multiple entities. The core of this path is to build an innovative ADMM-IPM hybrid framework. This framework first performs differentiated modeling on multiple market entities, supporting the detailed response characteristic characterization of no less than six types of entities. At the solution level, a hierarchical architecture of "external decomposition and internal refinement" is adopted: ADMM is used to achieve distributed coordination across regions and markets to ensure decision-making autonomy. For each sub-problem, an improved IPM is used to accurately solve the optimal power flow, including AC power flow constraints to ensure high accuracy and physical feasibility of the solution. The main kernel innovation of this paper is to establish a full-time safety closed loop, turning the conventional offline passive safety checking into a real-time active feedback procedure strongly coupled with the optimization process. The results of verification can correct the penalty parameters dynamically and drive re-optimization, and as such close-loop control of "optimization-verification-correction" can be pursued. The proposed algorithm module has been tested on benchmark systems as well as real power grids, and a solution based on this design has the potential to become a practical, economical, secure, and computationally efficient engineering approach for electric spot markets involving a large-scale integration of renewable energy sources.

2. Joint Clearing Model based on ADMM-IPM Hybrid Framework

Fig. 1 shows the basic framework structure of the hybrid ADMM and IPM algorithmic solution. Through multidimensional response characteristics, the multi-market entity module is interfaced with the ADMM coordination layer, enabling the distributed solution. The coordination layer obtains the coordination decomposition across multiple trading products over multiple regions, via globally consistent variables. Regional and trading sub-problems create a dual layer of parallel computations. Each sub-problem is solved by an IPM solver, and the physical feasibility of solutions is guaranteed by the embedded safety constraints. A safety verification system and feedback mechanism that constitute a closed-loop control loop, which adaptively changes the penalty parameters to lead to system convergence. The whole procedure reflects the deep integration of decomposition and coordination with high solution precision, which could be regarded as a systematic approach for joint clearing of the electricity market that integrates economic efficiency, security and computation efficiency.

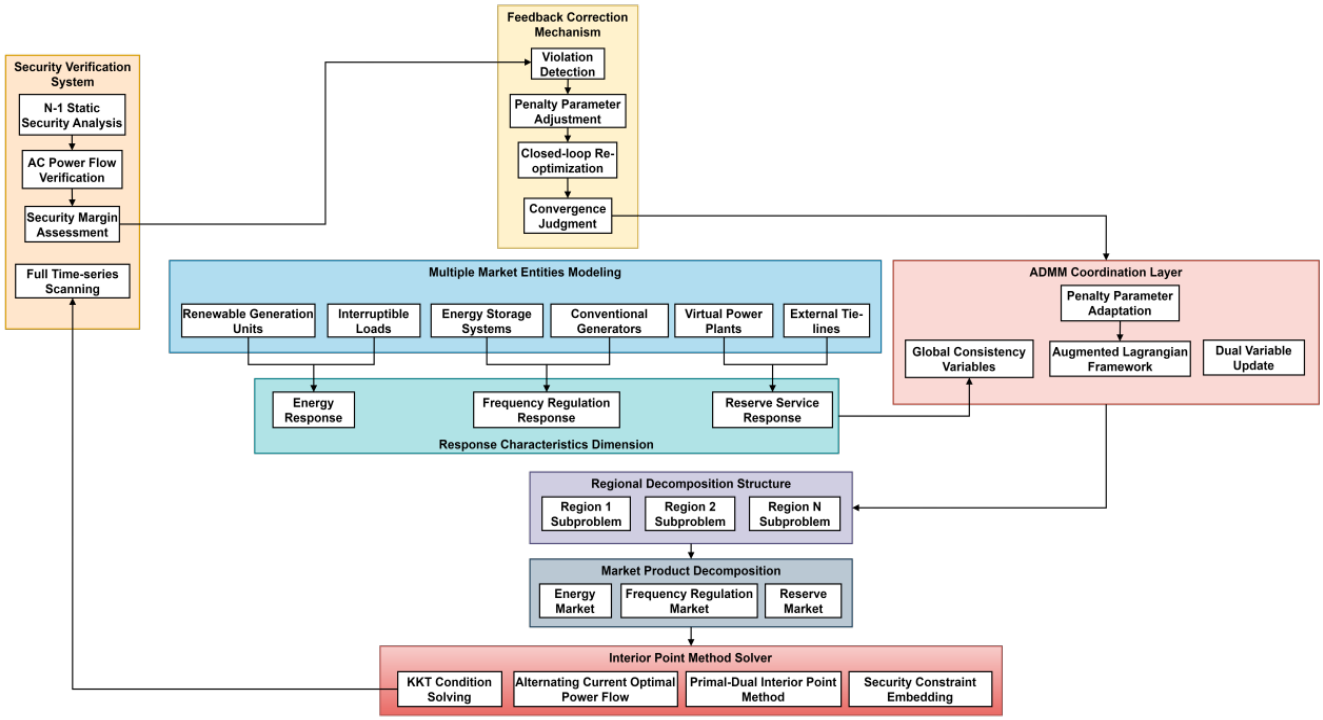

Fig. 1. Core structure of the hybrid ADMM and IPM framework

2.1. Multi-Agent Modeling and Problem Decoupling for Joint Clearing

2.1.1. Multi-agent multi-dimensional response characteristic modeling and structured constraint expression

The dynamic response capabilities of six core market entities include new energy generation units, energy storage devices, virtual power plants, interruptible loads, conventional units, and inter-regional interconnectors. In terms of power generation, frequency regulation, and backup services are analyzed to address the heterogeneity of the participating entities in the new power system. Based on its physical mechanism and operating boundaries, a cost function and a feasible domain constraint set with time-coupling characteristics are constructed. New energy power generation units should introduce power prediction confidence intervals, such as output upper limit constraints, embedded ramp rate limits and wind curtailment penalty terms and reflect their uncertainty and scheduling rigidity. Energy storage devices establish a time-series correlation model using

charge and discharge state transition equations, thereby clarifying the maximum number of cycles, the charge-state safety interval, and the efficiency attenuation factor, ensuring energy conservation and equipment life are compatible throughout the entire cycle. As a whole, the virtual power plant adopts a hierarchical response coefficient allocation mechanism to integrate its internal resource response potential into an equivalent output curve based on priority weighting and sets a response delay time window to reflect the lag effect of the control link.

In the dimension of auxiliary services, the frequency regulation service modeling focuses on the frequency deviation suppression capability, sets the adjustable capacity boundary based on the inertia constant and the primary frequency regulation dead zone, and converts the response speed index into a power change rate constraint on the time ladder. The standby service distinguishes between rotating and non-rotating types. The former requires the unit to retain an upward adjustment margin and meet the callable conditions within 10 minutes. The latter is defined jointly by the available transmission capacity of the external interconnection line and the interruptible capacity on the load side. The cost function of each entity adopts a piecewise linearized quadratic structure, taking into account both computational tractability and economic signal accuracy, and its form is as shown in Eq. (1).

$$C_i\left(p_i^e,p_i^d,p_i^a\right)=\alpha_i\left(p_i^e\right)^2+\beta_i p_i^e+\gamma_i+\lambda_i^d p_i^d+\lambda_i^a p_i^a \tag{1}$$

C_i represents the comprehensive cost of the i-th entity; p_i^e, p_i^d, p_i^a represent their declared outputs for electric energy, frequency regulation, and backup services, respectively. α_i, β_i, γ_i represent their energy cost parameters, λ_i^d and λ_i^a represent the bids for ancillary services. This cost structure explicitly separates the economic signals of electricity and ancillary services, avoiding cross-subsidies and ensuring financial transparency in multi-service bidding.

2.1.2. Decoupling decision variables and sub-problem structure generation

Structural decomposition is used to implement high-dimensional joint decision-making solutions. Based on the dual dimensions of transaction type and geographic region, the global variable P in the original problem are split into several mutually exclusive and complete subsets $P_{k,r}$, where the subscript $k\in\{e, d, a\}$ identifies the transaction type (energy, frequency regulation, or reserve), and r represents the region number. Each subset contains only the output decision variables and interface exchange volume for the corresponding region in a specific market, thus achieving logical isolation of the variable domain. Furthermore, cross-regional tie line power, node marginal prices, and ancillary service capacity are identified as consistent coupling variables. These are removed from the local decision set and instead serve as information exchange in the ADMM coordination layer.

Furthermore, based on ownership relationship and network topology partitioning, the market entities in each region are classified into corresponding sub-problem modules according to service type, ensuring that each sub-problem maintains the integrity of independent modeling and solution. The variable division process strictly follows the principle of "local controllability and boundary transmission": all local control variables within the region are retained in the sub-problem, while variables involving cross-regional balance or market linkage are loosely coupled via Lagrange multipliers and penalty terms. The final sub-problem structure meets the three engineering requirements of convexity maintenance, strong sparsity, and communication load balancing. Its form is as shown in Eq. (2).

$$\min_{x_{k,r}} \sum_{i\in G_{k,r}} C_i\left(x_i\right) \quad \text{s.t.} \quad g_{k,r}\left(x_{k,r}\right)\leqslant 0, \quad h_{k,r}\left(x_{k,r}\right)=0 \tag{2}$$

$x_{k,r}$ is the decision vector for the r region in the k transaction. $G_{k,r}$ represents the set of entities belonging to this sub-problem. $g_{k,r}$ and $h_{k,r}$ represent inequality and equality constraint functions, respectively, encompassing physical and market rules such as equipment output limits, power balance, and backup redundancy. This sub-problem structure decomposes the globally coupled problem into locally controllable units, laying the foundation for parallel solution and regional autonomous decision-making.

2.2. ADMM Distributed Solution Framework for Multi-Market Collaboration

2.2.1. Definition of multi-market coupling variables and development of augmented Lagrangian framework

Common, consistent variables across markets are then identified to enable coordinated optimization of energy, frequency regulation, and reserve transactions in a single clearing problem. Based on this, a mathematical framework for the distributed solution is derived. The node marginal electricity price, the frequency regulation capacity allocation factor and the regional reserve sharing parameter are considered as common variables across the submarkets. These values must be equal across the different trading sub-problems and define the key subsystems at the core of multi-type cooperative decision making. Separate sub-optimizations for each trading type are created. The objective function minimizes the overall cost of the corresponding market, and the constraints include local unit output capacity, service response timing characteristics, and network static security boundaries. Furthermore, consistency constraints are introduced to enforce convergence of solutions for each submarket on these common variables. Based on this, an augmented Lagrangian function with a penalty term is constructed as the optimization carrier for the coordination layer. Its form is as shown in Eq. (3).

$$L_\rho=\sum_{k\in\{\varepsilon,r,a\}}\left(f_k\left(x_k\right)+\lambda_k^T\left(z-A_k x_k\right)+\frac{\rho_k}{2}\left\|z-A_k x_k\right\|^2\right) \tag{3}$$

$f_k(x_k)$ represents the objective function of the k-type trading sub-problem, x_k represents its local decision variable vector, and z represents the set of globally consistent variables (i.e., node electricity prices, frequency regulation allocation coefficients, and reserve sharing thresholds). A_k is the mapping matrix used to align the local variable space with the global variable space; λ_k is the corresponding Lagrange multiplier, reflecting the marginal price signal of resource competition

between markets. ρ_k is the ADMM penalty parameter, controlling the penalty for deviations from the global consensus. The augmented Lagrangian function enforces consensus across sub-markets on key variables, such as nodal electricity prices and frequency regulation allocation coefficients, via a quadratic penalty term, thereby achieving cross-market resource coordination and price convergence. This formulation transforms the original high-dimensional coupled problem into multiple sub-problems that can be processed in parallel, while enhancing the stability of the iterative process using quadratic penalties.

2.2.2. Inter-regional liaison and coordination mechanism and two-level alternating update process

In the cross-regional joint clearing scenario, the ADMM coordination architecture is further extended to support distributed computing across geographical regions. Using regional interconnection line transmission power and section congestion status as cross-region coupling variables, these variables are incorporated into the global consensus variable set, forming a decomposition structure with a dual "transaction-region" dimension. After each transaction, the sub-problem within each region is solved locally, and its optimal response with respect to the variable set is uploaded to the central coordinator, which then forms a response as shown in Eq. (4).

$$z^{(t+1)}=\underset{z}{\operatorname{argmin}} \sum_{k,r} \left\|z-A_{k,r}x_{k,r}^{(t)}\right\|_{\rho_{k,r}}^{2} \tag{4}$$

This step essentially performs a weighted projection of the local solutions output by all sub-problems to generate a global consensus solution for the current iteration, where $x_{k,r}^{(t)}$ represents the local solution for the tth generation of the rth region in the kth type of transaction, and the weight is determined by the penalty parameter $\rho_{k,r}$. This update rule generates a global consensus value by weighted averaging of the local solutions of each sub-problem, reflecting the fairness and stability of information aggregation under a distributed architecture. Subsequently, the central coordinator sends the updated $z^{(t+1)}$ to each sub-problem unit to modify the dual variables in the next stage. Its form is as shown in Eq. (5).

$$\lambda_{k,r}^{(t+1)}=\lambda_{k,r}^{(t)}+\rho_{k,r}\left(z^{(t+1)}-A_{k,r}x_{k,r}^{(t+1)}\right) \tag{5}$$

The trade-off is that it creates a decoupled transfer of information between markets and regions, which prevents exposing the original data set to risk. The update procedure is performed in a synchronous iterative manner, i.e., all the sub-problems are solved simultaneously at each main-layer iteration, thus the computational load is well-balanced. Tie-line power errors are also directly included in the convergence tests. Now consider the case when the relative change rate of every interface variable in two successive iterations is less than a predetermined threshold, and the dual residuals are less than the tolerance, which means the system is taken to have attained a coordinated equilibrium. This process separates the local vs global decision-making conflict and makes possible very efficient joint clearing with multiple large scale entities participating.

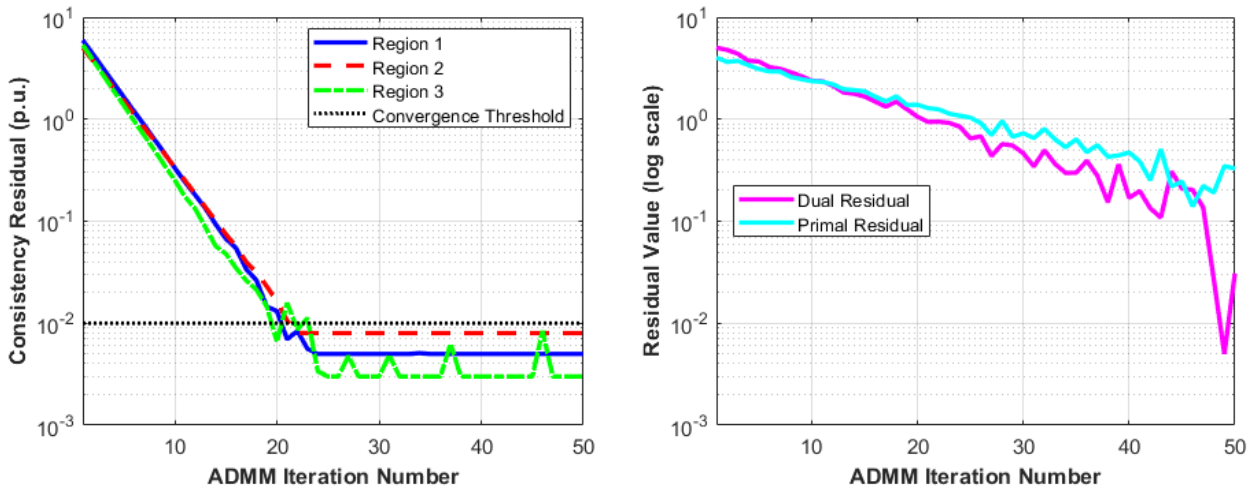

(a) Multi-region consistency residual convergence (b) Dual vs prime residual convergence

Fig. 2. ADMM convergence performance analysis

The convergence properties of ADMM in Fig. 2 mainly illustrate the nature of the dynamics in the multi-regional power market cooperative optimization. Figure 2(a) takes three distinct regions as an example and illustrates the decay curve of the consistency residual as the number of iterations increases. Variance in the rate of convergence across regions is attributed to the response characteristics of the market participant, including network topology complexity and heterogeneous response characteristics. Region 3 is comparatively low because its power balance is simple; regions 1 and 2 also drop below the cutoff later. Fig. 2(b) plots the dual residual and the primal residual, which form the dual condition of convergence of the algorithm. The dual residual also decreased fast, confirming that the Lagrange multiplier propagates the marginal price signals between regions effectively, dropping later to below 0.1. The relatively steady decrease of the primal residual is interpreted as the progressive achievement of the satisfaction of the physical operational constraints. Both curves have low residual values for late-stages iteration, implying the economics and physical safety are in good balance. This convergence

pattern is, in essence, the external manifestation of the coupling between local decision-making and global coordination in distributed optimization. Each region can reach an optimal resource allocation with a finite number of information exchanges.

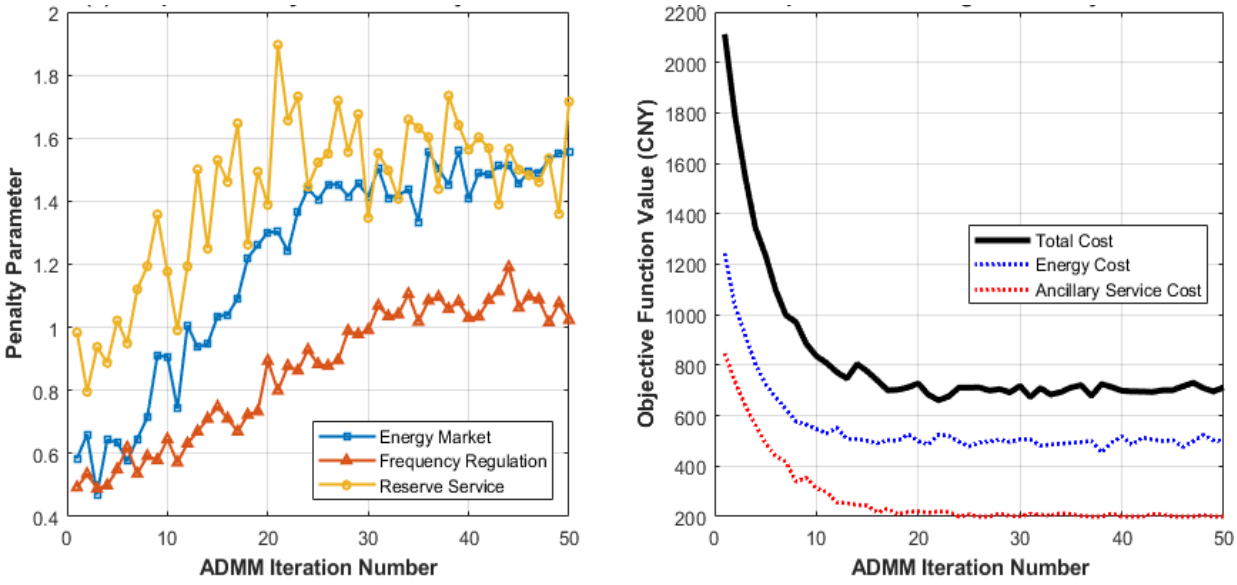

(a) Adaptive penalty parameter adjustment (b) Decomposition convergence of objective function

Fig. 3. ADMM convergence: penalty parameters and objective function

The process of adaptively updating the ADMM penalty parameters is shown in Fig. 3(a). The energy market parameters rise rapidly at the beginning and then become stable, since they are highly subject to global consistency constraints during the early coordination steps. The frequency regulation service parameters change at a moderate speed to reflect their fast response and smaller local decision space. The backup service parameters have substantial fluctuations because of the uncertain environment in which they operate as a security system cushion. This differentiated tuning strategy stands for the profound physical meaning embedded in the multiple markets of the algorithm, thus attaining an appropriate tradeoff between computational efficiency and convergence accuracy by means of the dynamic parameter's readjustment. Fig. 3(b) illustrates the evolution of the objective within the decomposed coordination framework of convergence. The total cost curve shows a typical decay curve. The early fast descent reflects a resolution in a coordinated fashion of the main conflicts among the sub-problems, while the slow convergence phase (under 800 CNY) presages a slow trajectory of somewhat localized refinements. The rates of convergence for energy costs and ancillary service costs are different: the former is relatively slow due to network constraints, but the latter is fast and robust due to smaller decision-making dimensionality. This layered convergence stems from the structural nature of an integrated Stockholm electricity market, as every sub-system tends to global best solutions at different speeds according to the complexity of its physical constraints.

2.3. High-Precision and Secure Embedded IPM Solutions at Sub-Problem Level

2.3.1. AC optimal power flow modeling and primal-dual IPM iterative solution

For each sub-problem decomposed from the ADMM, a nonlinear optimal power flow model is constructed with the goal of minimizing active power output regulation costs. Its constraint system fully encompasses the AC power balance equation, node voltage amplitude bounds, branch thermal stability limits, and generator reactive output capacity. Decision variables include the active and reactive outputs of all controllable units in the region, node voltage phase angles and amplitudes, and tie-line transmission power. The AC power flow equation in polar coordinates serves as the core equality constraint to ensure physical feasibility. Its form is as shown in Eqs. (6) and (7).

$$P_i = \sum_{j \in N_i} V_i V_j \left(G_{ij} \cos\theta_{ij} + B_{ij} \sin\theta_{ij} \right) \tag{6}$$

$$Q_i = \sum_{j \in N_i} V_i V_j \left(G_{ij} \sin\theta_{ij} - B_{ij} \cos\theta_{ij} \right) \tag{7}$$

P_i and Q_i are the net injected active and reactive power at the node, respectively. V_i and V_j are the voltage amplitudes at the corresponding nodes, θ_{ij} represents the phase difference between nodes, G_{ij}, B_{ij} are admittance matrix elements, and N_i represents the set of adjacent nodes connected to the node. Inequality constraints explicitly introduce the line active power flow upper limit $|S_{ij}| \leqslant S_{ij}^{max}$, the voltage operating range $V_i^{min} \leqslant V_i \leqslant V_i^{max}$, and the unit reactive response boundary $Q_i^{min} \leqslant Q_i \leqslant Q_i^{max}$. This set of AC power flow equations fully characterizes the nonlinear physical relationship among active/reactive power, voltage amplitude, and phase angle, and serves as the core constraint ensuring the grid feasibility of the solution.

The primal-dual IPM is used to solve this nonlinear programming problem. The inequality constraints are transformed into a continuously differentiable form by introducing slack variables and barrier functions, and a Karush-Kuhn-Tucker (KKT) conditional system is constructed. The augmented KKT system of equations is linearized and iterated using the Newton-Raphson method, with the primal variables, dual multipliers, and complementary gap parameters updated

simultaneously with each step. The search direction solution process leverages the sparsity structure of the Jacobian and Hessian matrices, employing a multi-prefix Lower-Upper (LU) decomposition to accelerate the solution of the linear system, ensuring numerical stability and convergence efficiency even in high-dimensions. The iteration termination condition is set to ensure that the dual residual, primal residual, and complementary gap are all below the 10^{-6} level, ensuring that the solution accuracy meets engineering application requirements.

2.3.2. Dynamic safety margin correction and online objective function feedback mechanism

During each major iteration of the original dual IPM, a real-time safety state assessment module is embedded to perform over-limit scanning on critical sections under the current power flow solution. After obtaining the transient voltage amplitude and branch apparent power, the load factor index $\eta_{ij}=|S_{ij}|/S_{ij}^{max}$ of each transmission element is calculated, and branches with overload risk $\eta_{ij}>\eta_{thres}$ are identified. For such lines, instead of directly removing them or tightening hard constraints, the safety margin deficiency is converted into an additional penalty term and dynamically injected into the original objective function, forming an adaptive correction mechanism. The following extended objective function is constructed. Its form is shown in Eq. (8).

$$\tilde{f}(x)=f(x)+\sum_{(i,j)\in L_{crit}} w_{ij}\cdot\max\left(0,|S_{ij}|-\alpha_{ij}S_{ij}^{max}\right)^2 \tag{8}$$

In Eq. (8) $f(x)$ is the original cost function, L_{crit} represents the set of currently detected high-risk lines, and w_{ij} is the dynamic weight coefficient, reflecting the branch's priority in system safety. α_{ij} is the preset safety reserve ratio, and max ensures that penalties are triggered only when the actual power flow exceeds the adjusted limit. This quadratic term is incorporated into the IPM objective function reconstruction and used to update the Hessian matrix, allowing subsequent iterations to proactively avoid high-stress areas.

This feedback process is executed once per IPM outer iteration, providing coupled guidance between the safety verification and the optimization path. w_{ij} is increased stepwise based on the number of violations in consecutive iterations, strengthening the suppression of stubborn violations. When a line no longer triggers penalty conditions for three consecutive rounds, its weight is restored to its initial value to avoid excessive interference with economic objectives.

Table 1. IPM core parameter configuration

	Value	Description
Voltage Magnitude Lower Bound	0.95	Minimum permissible p.u. voltage at nodes
Voltage Magnitude Upper Bound	1.05	Maximum permissible p.u. voltage at nodes
Branch Power Threshold	0.95	Load factor triggering security check
Security Margin Ratio	0.9	Reserved capacity ratio for thermal lines
Initial Penalty Weight	100	Starting weight for constraint violation
Weight Increment Step	50	Step size for penalty coefficient update
Maximum Iteration Count	30	Upper limit of interior-point outer loops
Dual Residual Tolerance	1e-6	Convergence criterion for dual feasibility
Primal Residual Tolerance	1e-6	Convergence criterion for primal feasibility
Complementarity Gap Tolerance	1e-6	Termination threshold for optimality gap

Table 1 presents the parameters for the sub-problem IPM solution and the process of embedding safety. The operating voltage limits can be viewed as the node potential feasibility region, and the branch load constraints correspond to potentially violated components. A safety margin factor provides redundancy in the transmission capacity, and a dynamic penalty weight scheme is applied to direct power flow redistribution based on feedback from the objective function. A stopping rule is imposed to control the computational accuracy of the NLP solution, and a maximum number of iterations is allowed. The parameter system enables AC-constrained compact modeling, which strikes a good balance between the optimization efficiency and physical feasibility, and serves as the basis for the high-precision local solutions.

2.4. Full-Time Sequence Safety Closure and Adaptive ADMM Parameter Adjustment

2.4.1. Time sequence section safety verification trigger mechanism

The full-time security check is immediately called after the ADMM main iteration for 96 daily time intervals. Given the unit output, tie-line schedule, and network topology at each time interval, a baseline power flow model for the respective operating mode is constructed. An N-1 static security check is conducted with this model. The validation is performed on all trunk lines, critical buses, and inter-regional transmission links, one at a time, and each vulnerable component is removed to analyze the post-fault load-power system distribution. A fast decomposition method based on the DC sensitivity pre-screening method is used to preliminarily screen out unfeasible branches with overload hazards. Then the AC power flow is precisely computed for those candidate sections to verify voltage and thermal stability breaches.

A two-part test is introduced: (1) if the apparent power of a branch (at the matched end) under an N-1 contingency scenario is greater than the 105% of its thermal stability margin. (2) If the voltage magnitude deviation at a node is more than 8% of its rated value, the safety verification of the stage is regarded as failed. The verification results are labeled by region r and time period t, generating a binary discriminant matrix $\delta_{r,t} \in \{0,1\}$, where $\delta_{r,t}=1$ indicates an unacceptable safety hazard in the region r at time t. This matrix serves as a trigger for subsequent correction logic, activating the revised optimization path for the corresponding sub-problem only when $\delta_{r,t}=1$ occurs, avoiding resource waste caused by indiscriminate recalculation. The entire verification process is embedded in a parallel computing architecture that leverages data independence across time periods to enable batch processing across time dimensions, ensuring that a full 96-point cycle analysis can be completed within minutes.

2.4.2. Adaptive Penalty Parameter Adjustment and Closed-Loop Revised Optimization

For the time period and regional pairs that are at risk, a dynamic ADMM penalty parameter modulation approach based on safety margin feedback is proposed. The initial penalty factor is progressively increased following the verification violation, with the following update rules. Its form is as shown in Eq. (9).

$$\rho_{k,r,t}^{new}=\rho_{k,r,t}^{old}\cdot\left(1+\beta\cdot\max_{(i,j)\in E_{r,t}}\left(\frac{|S_{ij}|}{S_{ij}^{max}}-1\right)^{+}\right) \tag{9}$$

$E_{r,t}$ is the set of devices that violated limits within the region r during that period. $(\cdot)^{+}$ represents the non-negative portion, and β is the gain factor, which controls the magnitude of the adjustment. This formula ensures that the penalty increment is positively correlated with the most severe violation, preventing overly aggressive parameter jumps. The updated $\rho_{k,r,t}$ is incorporated into the augmented Lagrangian function of the corresponding sub-problem, enhancing the tracking rigidity of its local solution to the global consistency variable, forcing subsequent iterations to more strictly meet cross-region power balance and interface capacity constraints. This adaptive rule dynamically increases the penalty intensity based on the severity of safety violations, enhancing the ADMM's ability to exclude infeasible solutions and accelerating convergence to the safe, feasible region.

After the parameter update is complete, the ADMM main-layer coordination process for that period is restarted, re-executing the sub-problem solution, consistency variable update, and dual ascent steps. This re-optimization process is limited to a maximum number of iterations, T_{max}, to prevent infinite loops. If $\delta_{r,t}$ returns to 0 within the specified number of rounds, the correction is considered successful. Otherwise, the current optimal feasible solution is retained, and a warning flag is recorded. All periods that pass the verification have their clearing results frozen and are no longer subject to subsequent adjustments.

3. Case Study Analysis: Comprehensive Verification of the Hybrid Clearing Algorithm Performance

3.1. Experimental Setup

The simulation data and the scenario settings are designed for practical application, enabling full verification of the proposed ADMM-IPM hybrid framework in a realistic electricity market environment. All the cases are modeled on a testbed that combines the modified IEEE 500 system with real data from a provincial power grid in China.

Modeling six market players, renewable energy generation units (wind and photovoltaic), energy storage devices, Virtual Power Plants (VPPs), interruptible loads, conventional thermal power units, and interregional interconnectors, is taken into account in the proposed model. Its cost behavior and its response are derived from historical bids and physical constants. The renewable energy output curve is generated using a high-precision meteorological forecast model and superimposed with a ±15% confidence interval to account for uncertainty. The energy storage system's state of charge is initially set to 50%, accounting for its charge and discharge efficiency and lifetime degradation constraints. The VPP aggregates distributed resources, and its responsiveness is determined based on the agreed flexibility range in the contract.

In terms of market scenario settings, this paper designed a multi-dimensional comparative experiment. First, 96 time slices were used to simulate the complete day-ahead market cycle. Second, regarding system state, three scenarios of renewable energy installed capacity penetration (20%, 35%, and 50%) were used to evaluate the algorithm's adaptability to the low-carbon transition. Finally, the RobustNES algorithm was verified at three levels of uncertainty in the disturbance size (±5%, ±10%, and ±15%), with step-wise load variations in the disturbance size. The same market rules, network parameters and random seeds were used to run all competing algorithms, which ensured the comparison results were fair and valid.

3.2. Co-Analysis of Multi-Agents Operational Constraints and Cost Features

Considering dynamic meteorological conditions and unit operating state, a day-ahead forecast curve with a confidence interval is provided. The dispatch process, which is based on the grid security regulations, also has ramp rate and capacity limits for safety verification and modification of the forecast power. The ESS assessment adopts field operation data to develop a charge/discharge efficiency model considering battery aging. Based on historical load and market-clearing outcomes, energy storage operating policies are reformulated. SOC dynamics are modeled by fitting real operating data, and the charge and discharge behaviors are associated with real-time electricity prices and ancillary service demand signals. The whole procedure integrates physical limitations and market mechanisms and utilizes multi-source data cross-validation to make the analysis of response characteristics in engineering feasible.

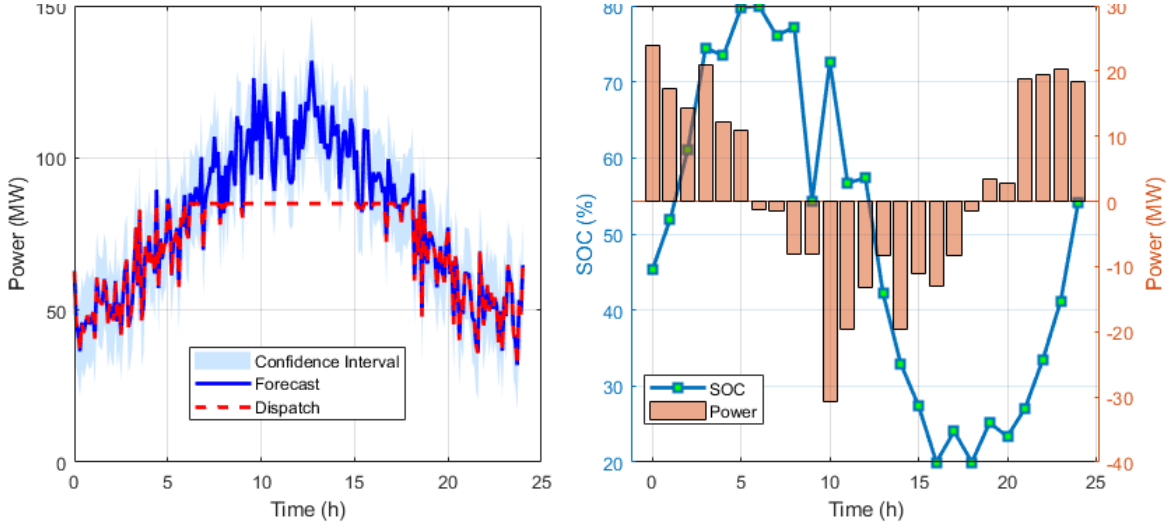

(a) Wind power unit (b) Energy storage system

Fig. 4. Operational characteristics and inherent constraints of multiple entities

In Fig. 4 is a summary of the operation and physical constraints of various electricity market participants along several dimensions. Fig. 4(a) illustrates the gap between the predicted wind turbine power and the dispatched power. The solid blue line is the theoretical power generation potential from the meteorological field, the dashed red line is the dispatch range permitted by the ramp rate and capacity constraints, and the shaded light blue region is the forecast uncertainty band. The periodic fluctuations of wind power are caused by the natural distribution of temporal wind resources, and the processing of the dispatching curve expresses strong restrictions on the changing rate of power for safe system operation, which is rigid. Fig. 4(b) illustrates the performance of the Energy Storage System (ESS) under its potential dual role as energy time shifting and power regulation. The State of Charge (SOC) plot on the left depicts cyclical charge-discharge behavior, and its operating region is constrained between 20% and 80%. This design is from the perspective of battery life management and safe operation. The energy storage system power bar on the right shows the frequency load pattern of the energy storage system's power output during peak load hours. The magnitudes of charge and discharge power vary and illustrate its capacity to switch seamlessly between the electricity and ancillary services markets. The trajectory of the Energy Storage System (ESS's) operations is also influenced by electricity price signals, as well as by frequency regulation and backup calls. The dynamic evolution of its SOC is essentially the integrated effect of multiple market signals over time.

The approach starts by forming a primary cost function with the energy output and reserve capacity as decision variables. A 2D discrete grid is constructed from the real operating domain. The total cost is computed for each point in the grid, with the energy and reserve parameters being sampled gradually in their intervals. The economic cost of each pair is stored. After the calculations are done for all points, the cost values are normalized to remove the dimensionality effects.

Fig. 5 presents the cost distribution of a typical entity under the dual variables of energy output and reserve capacity. The normalized values on the horizontal and vertical axes represent the energy range from zero to maximum rated output and the proportion of reserve capacity within its maximum adjustable range. Costs rise rapidly with increasing energy output, while the cost increase with increasing reserve capacity is more gradual. The difference in the slope of the surface indicates that, for entities of the same size, the marginal cost of energy output is much higher than the economic cost of reserve capacity. This is closely related to the unit's ramping capability, thermal efficiency, and operational constraints. The overall upward trend of the cost surface indicates that the system's costs cannot experience unphysical cost reductions under full-scale operation, and each point corresponds to a feasible unit combination. The varying directions of change reflect the varying influences of energy and ancillary services on economic load allocation, enabling the sub-problem to adjust output strategies based on cost responses during the iteration process without relying on additional linearization assumptions or mandatory constraints.

3.3. Solution Efficiency Analysis in Multiple Scenarios

On a 500-node system, this paper tested the total solution time (unit: seconds) and the average number of iterations for the ADMM-IPM compared with the classic ADMM independent solver, the Benders decomposition method, the Alternating Minimization (AM) method, and the Proximal Gradient Method (PGM). The simulation was repeated 30 times under three load fluctuation scenarios: ±5%, ±10%, and ±15%. The mean and standard deviation of the solution time for each method were calculated to evaluate its stability.

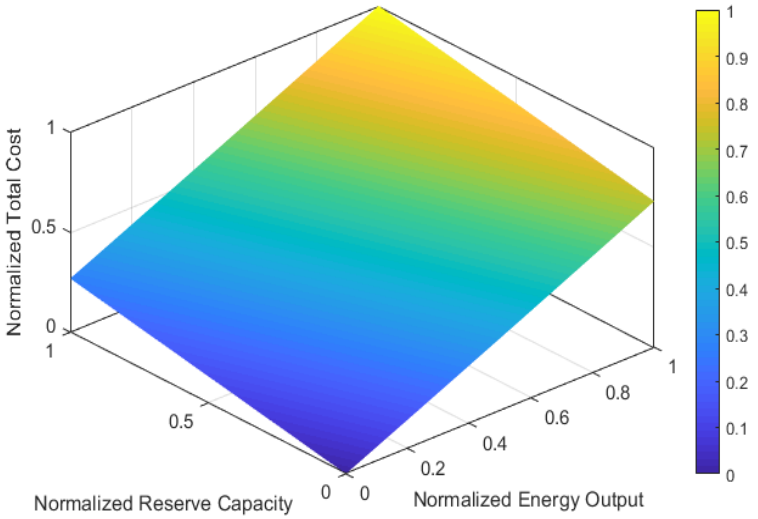

Fig. 5. Typical entity cost surface

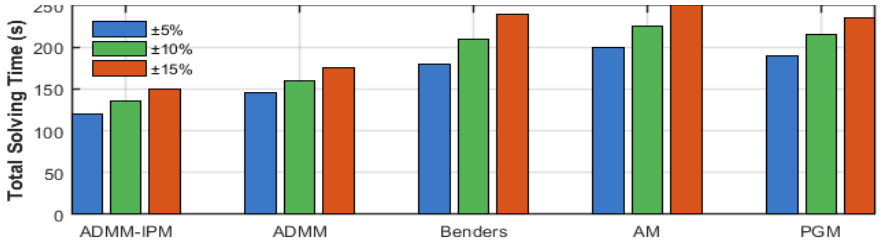

(a) Comparison of total solving time

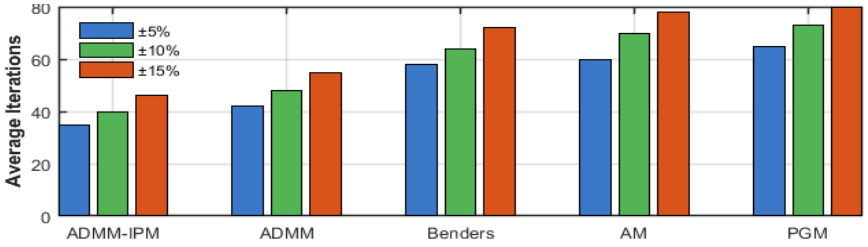

(b) Comparison of average iteration count

Fig. 6. Performance evaluation under multiple load fluctuations

Fig. 6 compares the computational performance of different solution algorithms under multiple load fluctuation scenarios. Fig. 6(a) shows how total time varies with system disturbance intensity. ADMM-IPM maintains the lowest time consumption across all three levels of fluctuation, with a total solution time of only 150 seconds at a ±15% load fluctuation. Its high-precision convergence of sub-problems effectively suppresses ineffective iteration expansion. Traditional ADMM suffers from significant latency due to insufficient accuracy in the inner layer. Bender's decomposition is constrained by the information exchange bottleneck of the master-slave structure, limiting its response speed. AM and PGM, due to the accumulation of gradient estimation errors, fall into a slow convergence region in high-dimensional nonlinear environments. Fig. 6(b) shows the average number of iterations. ADMM-IPM maintains the lowest value and increases slowly. Under a fluctuation of ±15%, the average number of iterations is only 46. This is attributed to IPM's strong ability to handle nonlinear constraints and its proactive guidance of the feasible domain through its safety correction mechanism. As load fluctuations intensify, the number of iterations for each method generally increases, but the centralized algorithm's growth slope is significantly higher than that of the distributed architecture. Overall stability is optimal under the ±5% load condition, while decentralized characteristics increase at ±15%, reflecting the weakening effect of uncertainty on coordination efficiency. The global title uniformly depicts the test environment, and the horizontal axis is organized by algorithm category to ensure clear comparison logic.

3.4. Economic Performance at Different Penetration Rates

Three typical power structure scenarios were constructed, with the proportion of new energy installed capacity set at 20%, 35%, and 50%, respectively, to simulate the power system's low-carbon evolution path. Under each structure, the ADMM-IPM hybrid solution framework proposed in this paper and the four comparative algorithms of ADMM, Bender's

decomposition, AM and PGM were run to obtain the clearing results of each scenario. The core evaluation indicators are the proportion of the total electricity purchase cost and the ancillary service procurement cost (ASC) in the total cost. The total electricity purchase cost covers the energy expenditure of all winning units and the total payment for frequency regulation and standby services, reflecting the overall economic burden. The proportion of ancillary service costs is used to measure the additional adjustment cost paid by the system to cope with uncertainty, indirectly reflecting the efficiency of resource allocation. By comparing the cost trends of different approaches as penetration rates increase, this paper assesses their compatibility with market incentives and adaptability to high levels of renewable energy penetration. All simulations maintain consistent load levels, network parameters, and bidding strategies, ensuring that cost differences stem solely from the optimization mechanism's resource allocation characteristics. The calculations incorporate voltage safety constraints and N-1 verification feedback to ensure the physical feasibility of the solutions.

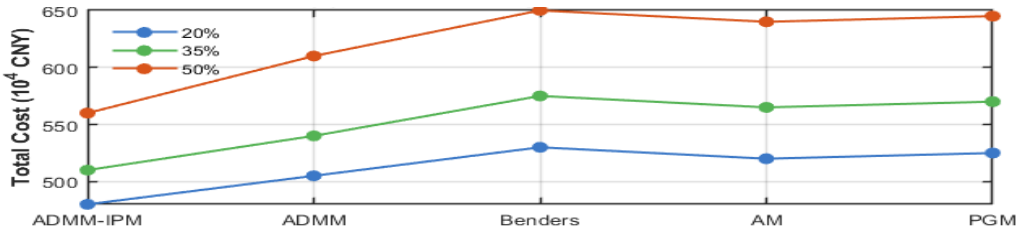

(a) Total electricity procurement cost

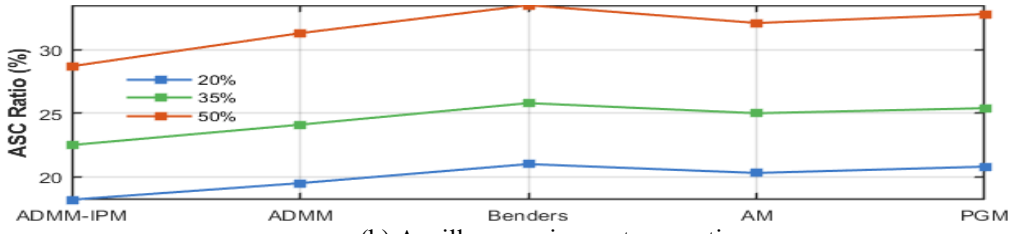

(b) Ancillary service cost proportion

Fig. 7. Economic performance with increasing renewable energy penetration

Fig. 7 demonstrates the cost performance of different algorithms at different levels of renewable energy penetration. In Fig. 7(a), the increase in the total electricity purchase cost with increasing Renewable Energy (RE) penetration is depicted. The ADMM-IPM algorithm still achieves the minimal cost among the three schemes. The total cost of electricity purchase is 5.6 million yuan at a 50% renewable energy penetration rate. It's combined clearing ties together the marginal costs of energy and reserves, mitigating strategic bid price inflation. The system's uncertainty increases as the penetration rate ranges from 20% to 50%. Because of the disjointed safety verifications, conventional approaches bring about redundancy in the acquisition of regulatory resources and lead to inflated costs. The information loss in Bender's decomposition leads to error-prone solutions in stochastic settings with high volatility. The AM and PGM methods are subject to the gradient deviation and thus cannot get arbitrarily close to the boundaries of non-convex feasible sets. Evolution of the AS cost percentage is illustrated in Fig. 7(b). At the 50% renewable energy capacity, the AS procurement cost ratio of ADMM-IPM is 28.7%. This is because IPM accurately handles AC constraints, eliminating unnecessary reserves.

3.5. Comprehensive Verification of Safety Constraint Closed-Loop Capabilities

After completing the basic clearing, the dispatch plans generated by the five methods were subjected to a full-time N-1 static safety check. The number of branches with excessive power flow and the number of nodes with excessive voltage were recorded. This paper further simulates a critical line disconnection event. Under the same rescheduling resource-pool conditions, this paper compares the adjustment in Megawatts (MW) required to achieve safe recovery from the initial solution and the revised optimization time (seconds) required for each method, reflecting their predictive control capabilities and safety robustness.

Table 2. Comprehensive verification of safety constraint closed-loop capabilities

Method	Branch Overload Count	Voltage Over-Limit Node Count	Rescheduling Adjustment (MW)	Revised optimization Time (s)
ADMM-IPM	2	1	147	9.3
ADMM	18	7	256	22.8
Benders	23	9	289	31.5
AM	20	8	274	26.4
PGM	25	11	302	35.7

Table 2 systematically evaluates the comprehensive performance of the five methods in safety constraint processing. ADMM-IPM outperforms the comparison algorithms in terms of branch overload (2) and voltage overrun (1) indicators. This is attributed to embedding the AC optimal power flow model in the sub-problem-solving stage and accurately capturing the nonlinear boundary using IPM, thereby making the initial clearing results more physically consistent. Traditional ADMM relies on DC approximation or simplified network models and fails to effectively predict the actual power flow distribution, resulting in many branch overruns. Benders, AM, and PGM ignore the dynamic reactive power and voltage coupling effects during the decomposition process, and the generated solutions deviate from the AC feasible domain. The number of rescheduling adjustments reflects the ability to proactively control. ADMM-IPM requires the smallest adjustment, indicating that its clearing solution proactively reserves sufficient safety margins, mitigating drastic resource fluctuations during emergencies. Revised optimization time depends not only on the efficiency of the algorithm itself but also on the proximity of the initial point to the feasible region. ADMM-IPM, thanks to its early closed-loop verification mechanism, maintains the post-fault state within a highly convergent region, significantly shortening recovery time. Overall, the data reveals that deeply integrating safety constraints into the optimization process, rather than verifying them post-failure, is a key path to improving the robustness of scheduling solutions.

3.6. Algorithm Scalability and Subject Compatibility Testing

As the system node size expanded from 200 to 1000, the memory usage growth slope (GB/100 nodes) and communication interaction data volume (MB/iteration) of this method were recorded when integrating six types of market entities (renewable energy generation units, energy storage devices, virtual power plants, interruptible loads, conventional units, and inter-regional interconnectors). The number of market entities also increased from 50 to 500, and the convergence success rates (number of successes/total number of runs) of the four methods were compared at different entity densities.

Table 3. Algorithm scalability and entity compatibility test

Market Entity Type	Memory Growth Slope (GB/100 nodes)	Communication Data Volume (MB/iteration)	Convergence Success Rate (50 units)	Convergence Success Rate (500 units)
Renewable Generation	0.38	1.24	1	0.96
Energy Storage Device	0.41	1.33	1	0.94
Virtual Power Plant	0.47	1.52	1	0.91
Interruptible Load	0.35	1.18	1	0.97
Conventional Unit	0.39	1.27	1	0.95
External Tie-line	0.33	1.12	1	0.98

Table 3 presents the performance response characteristics of the algorithm under the dual expansion of system scale and entity density. The memory growth slope reflects the marginal contribution of different market entities to computing resources. Virtual power plants, due to the aggregation of multiple sub-units and the inclusion of coordination constraints, have the highest storage overhead. The interruptible load and inter-regional interconnection line model has a simple structure and the corresponding lowest slope. The amount of communication data is positively correlated with the strength of variable coupling. Virtual power plants transmit equivalent output and flexibility boundaries between regions, resulting in a significant increase in interactive load. Energy storage devices are coupled across time periods due to their state of charge, and communication demand is secondary. The convergence success rate is used to measure numerical robustness under high-density access. All types achieve full convergence in the 50-unit configuration. As the number of agents goes up to 500, the non-convexity of the system increases, and some complex modeling objects present a very slight descending behavior. Virtual power plants have the biggest reduction as they are subject to a potential conflict between the priorities of the response of their internal resources and the external demands of the market. Renewable generation units and conventional units are highly stable because they are tightly defined by their physical nature, and the constraint structure is well-organized. In general, the proposed scheme is shown to be highly scalable and robust in a multi-agent coexisting environment, enabling continuous access to large-scale, diversified markets.

4. Conclusion

This paper develops a clear problem for electric energy and ancillary services for multiple entities and proposes an ADMM solution method. A dual decomposition of the transaction types and the regional dimension is used to exploit parallelization over the complex optimization problems, leading to improved scalability in terms of computation. The sub-problem uses a primal-dual IPM to accurately solve the AC optimal power flow and to improve the capacity to represent the limits on voltage, reactive power, and thermal stability. The safe constraints are integrated at the heart of iteration, and a closed-loop structure is formed where the verification results are fed back to adjust the optimization variables to make the solutions more physically feasible. The results for full-time N-1 verification and post-fault rescheduling reveal that the proposed method enjoys comprehensive superiority on initial plan security, reactive response sensitivity of disturbance, as well as regulation resource intensity. The algorithm enjoys favorable convergence when integrating new market entities, controls memory demands and communication load, and handles the simultaneous increase in system scale and in the number of participating entities. This balances the market-clearing economic objectives with the safety and robust requirements of grid

operation and offers a mathematically and engineering-sound technical solution for electricity spot markets with large-scale renewable energy integration.

This method has been validated on provincial power grid data and has the potential to be directly deployed in day-ahead market clearing systems, especially suitable for scenarios with a high proportion of renewable energy connected to the grid. However, the current framework assumes that market participants bids are given inputs and does not model strategic bidding behavior. Moreover, it relies on synchronous ADMM iteration, which may slow down convergence in asynchronous communication environments. Future work will introduce a reinforcement learning-based bid response model and explore event-triggered asynchronous coordination mechanisms to further improve the method's adaptability and robustness in real market environments.

Author Contributions

Xingyou Zhang contributed to conceptualization, methodology, investigation, data collection, and manuscript drafting; Yuanlong Liu contributed to methodology, validation, formal analysis, and manuscript reviewing and editing. Qiang Ma contributed to software development, data curation, and visualization. Shan Li contributed to the investigation, data collection, and preliminary analysis. Congcong Liu contributed to formal analysis, validation, and technical support. Jing Yao contributed to supervision, project administration, manuscript reviewing and editing, and correspondence with the journal. All authors have read and approved the final version of the manuscript and agreed to its submission and publication.

Funding

This work is supported by State Grid Shandong Electric Power Company's Scientific and Technological Project "Research on Key Technologies for Optimization and Improvement of Provincial-Level Electricity Spot Market Oriented to New-Type Power System" (52062625000P).

Institutional Review Board Statement

Not applicable.

Declaration of Artificial Intelligence (AI) Tools

The authors used Deepseek solely for language editing and readability improvement. The authors reviewed and verified all content and take full responsibility for the accuracy and integrity of the manuscript.

References

Alam, M. N., Khurshaid, T., and Rhee, S., B. (2024). Hybrid GA-IPM algorithm for optimal protection coordination of directional overcurrent relays with mixed time current characteristic curves. *Electrical Engineering,* 106(4), 5027-5041. https://doi.org/10.1007/s00202-024-02345-6

Antoniadou-Plytaria, K., Steen, D., Carlson, O., Mohandes, B., and Ghazvini, M. A. F. (2022). Scenario-based stochastic optimization for energy and flexibility dispatch of a microgrid. *IEEE Transactions on Smart Grid,* 13(5), 3328-3341. https://doi.org/10.1109/TSG.2022.3156789

Catalan, P., Wang, Y., Arza, J., and Chen, Z. (2023). A comprehensive overview of power converter applied in high-power wind turbine: Key challenges and potential solutions. *IEEE Transactions on Power Electronics,* 38(5), 6169-6195. https://doi.org/10.1109/TPEL.2022.3225678

Chen, S., Xu, C., Yan, Z., Guan, X., and Le, X. (2021). Accommodating strategic players in distributed algorithms for power dispatch problems. *IEEE Transactions on Cybernetics,* 52(11), 12594-12603. https://doi.org/10.1109/TCYB.2021.3123456

Chen, Y., Pan, F., Qiu, F., Xavier, A.S., Zheng, T., Marwali, M., Knueven, B., Guan, Y., Luh, P.B., Wu, L. and Yan, B. (2022). Security-constrained unit commitment for electricity market: Modeling, solution methods, and future challenges. *IEEE Transactions on Power Systems*, *38*(5), 4668-4681. https://doi.org/10.1109/TPWRS.2022.3223456

Costantini, G., and Görges, D. (2021). Fast distributed model predictive control combining ADMM, IPM and Riccati iteration. at-*Automatisierungstechnik,* 69(2), 97-110. https://doi.org/10.1515/auto-2020-0089

Dong, Y., Shan, X., Yan, Y., Leng, X., and Wang, Y. (2022). Architecture, key technologies and applications of load dispatching in China power grid. *Journal of Modern Power Systems and Clean Energy*, 10(2), 316-327. https://doi.org/10.35833/MPCE.2021.000432

Gholami, A., Sun, K., Zhang, S., and Sun, X., A. (2023). An ADMM-based distributed optimization method for solving security-constrained alternating current optimal power flow. *Operations Research,* 71(6), 2045-2060. https://doi.org/10.1287/opre.2023.2456

He, Q., Lin, Z., Chen, H., Dai, X., Li, Y., and Zeng, X. (2022). Bi-level optimization based two-stage market clearing model considering guaranteed accommodation of renewable energy generation. *Protection and Control of Modern Power Systems,* 7(3), 1-13. https://doi.org/10.1186/s41601-022-00250-8

He, X., Xiao, J. W., Cui, S,. C., Liu, X. K., and Wang, Y., W. (2021). A new cooperation framework with a fair clearing scheme for energy storage sharing. *IEEE Transactions on Industrial Informatics,* 18(9), 5893-5904. https://doi.org/10.1109/TII.2021.3123456

Hossain, M. B., Islam, M. R., Muttaqi, K. M., Sutanto, D., and Agalgaonkar, A. P. (2023). Dynamic electrical circuit modeling of a proton exchange membrane electrolyzer for frequency stability, resiliency, and sensitivity analysis in a power grid. *IEEE Transactions on Industry Applications,* 59(6), 7271-7281. https://doi.org/10.1109/TIA.2023.3298765

Huang, Y., Sun, Q., Li, Y., Zhang, H., and Chen, Z. (2022). Adaptive-discretization based dynamic optimal energy flow for the heat-electricity integrated energy systems with hybrid AC/DC power sources. *IEEE Transactions on Automation Science and Engineering,* 20(3), 1864-1875. https://doi.org/10.1109/TASE.2022.3201234

Jiang, K., Wang, P., Wang, J., and Liu, N. (2021). Reserve cost allocation mechanism in renewable portfolio standard-constrained spot market. *IEEE Transactions on Sustainable Energy,* 13(1), 56-66. https://doi.org/10.1109/TSTE.2021.3089123

Jiang, T., Wu, C., Zhang, R., Li, X., Chen, H., and Li, G. (2022). Flexibility clearing in joint energy and flexibility markets considering TSO-DSO coordination. *IEEE transactions on smart grid,* 14(2), 1376-1387. https://doi.org/10.1109/TSG.2022.3209876

Kiani, S., Sheshyekani, K., and Dagdougui, H. (2023). ADMM-based hierarchical single-loop framework for EV charging scheduling considering power flow constraints. *IEEE Transactions on Transportation Electrification*, 10(1), 1089-1100. https://doi.org/10.1109/TTE.2023.3301234

Levin, T., Bistline, J., Sioshansi, R., Cole, W.J., Kwon, J., Burger, S.P., Crabtree, G.W., Jenkins, J.D., O'Neil, R., Korpås, M., and Wogrin, S. (2023). Energy storage solutions to decarbonize electricity through enhanced capacity expansion modelling. *Nature Energy*, 8(11), 1199-1208. https://doi.org/10.1093/ce/zkaa045

Li, K., Guo, H., Feng, C., Yu, S., and Tang, Y. (2025). Modeling strategic behaviors of renewable-storage system in low-inertia power system. *Protection and Control of Modern Power Systems,* 10(5), 28-40. https://doi.org/10.23919/PCMP.2024.000200

Liu, Z., Huang, B., Li, Y., Sun, Q., Pedersen, T., B., and Gao, D. W. (2024). Pricing game and blockchain for electricity data trading in low-carbon smart energy systems. *IEEE Transactions on Industrial Informatics,* 20(4), 6446-6456. https://doi.org/10.1109/TII.2023.3321234

Lu, Z., Bai, L., Wang, J., Wei, J., Xiao, Y., and Chen, Y. (2022). Peer-to-peer joint electricity and carbon trading based on carbon-aware distribution locational marginal pricing. *IEEE transactions on power systems,* 38(1), 835-852. https://doi.org/10.1109/TPWRS.2022.3184567

Ma, H., Xiang, Y., Sun, W., Dai, J., Zhang, S., Liu, Y., and Liu, J. (2024). Optimal peer-to-peer energy transaction of distributed prosumers in high-penetrated renewable distribution systems. IEEE Transactions on Industry Applications, 60(3), 4622-4632. https://doi.org/10.1109/TIA.2024.3361234

Scolaro, M., and Kittner, N. (2022). Optimizing hybrid offshore wind farms for cost-competitive hydrogen production in Germany. *International Journal of Hydrogen Energy,* 47(10), 6478-6493. https://doi.org/10.1016/j.ijhydene.2021.12.123

Shelar, D., Amin, S., and Hiskens, I. A. (2021). Evaluating resilience of electricity distribution networks via a modification of generalized benders decomposition method. *IEEE Transactions on Control of Network Systems,* 8(3), 1225-1238. https://doi.org/10.1109/TCNS.2021.3067890

Tsaousoglou, G., Soumplis, P., Efthymiopoulos, N., Steriotis, K., Kretsis, A., Makris, P., Kokkinos, P., and Varvarigos, E. (2021). Demand response as a service: Clearing multiple distribution-level markets. *IEEE Transactions on Cloud Computing*, 10(1), 82-96. https://doi.org/10.1287/ijoo.2023.0089

Vera, E., G., Cañizares, C., A., Pirnia, M., Guedes, T., P., and Trujillo, J., D., M. (2022). Two-stage stochastic optimization model for multi-microgrid planning. *IEEE Transactions on Smart Grid*, 14(3), 1723-1735. https://doi.org/10.1109/TSG.2022.3212345

Wang, Q., Wu, W., Lin, C., Yang, Y., and Wang, B. (2023). A spatio-temporal decomposition method for the coordinated economic dispatch of integrated transmission and distribution grids. *IEEE Transactions on Power Systems*, 39(3), 4835-4851. https://doi.org/10.1109/TPWRS.2023.3312345

Wu, Z., Wang, J., Zhong, H., Gao, F., Pu, T., Tan, C.W., Chen, X., Li, G., Zhao, H., Zhou, M. and Xia, Q., 2022. Sharing economy in local energy markets. *Journal of Modern Power Systems and Clean Energy*, *11*(3), 714-726. https://doi.org/10.35833/MPCE.2022.000567

Xiao, H., Pei, W., Han, D., Pu, X., and Wang, J. (2024). Integrated energy microgrids participating in voltage regulation ancillary services: An improved ADMM based distributed optimization approach. *IET Renewable Power Generation*, 18(16), 4069-4083. https://doi.org/10.1049/rpg2.12876

Xing, H., Shen, J., Cheng, M., Zheng, Z., Shi, Y., and Luo, J. (2025). A Two-Stage Joint Clearing Model for Virtual Power Plant Participating in the Flexible Ramping Product Market Based on Chance-Constrained Programming. *Journal of Electrical Engineering & Technology,* 20(3), 1363-1382. https://doi.org/10.1007/s42835-024-02106-0

Yang, J., Dong, Z., Y., Wen, F., Chen, Q., and Liang, B. (2021). Spot electricity market design for a power system characterized by high penetration of renewable energy generation. *Energy Conversion and Economics*, 2(2), 67-78. https://doi.org/10.1049/cee2.12020

Zahedmanesh, A., Muttaqi, K., M., and Sutanto, D. (2021). A cooperative energy management in a virtual energy hub of an electric transportation system powered by PV generation and energy storage. *IEEE Transactions on Transportation Electrification,* 7(3), 1123-1133. https://doi.org/10.1109/TTE.2021.3055642

Zhang, D., Zhu, H., Zhang, H., Goh, H., H., Liu, H. and Wu, T. (2021). Multi-objective optimization for smart integrated energy system considering demand responses and dynamic prices. *IEEE Transactions on Smart Grid*, *13*(2), 1100-1112. https://doi.org/10.1109/TSG.2021.3112345

Zou, Y., Xu, Y., Feng, X., Naayagi, R., T., and Soong, B., H. (2022). Transactive energy systems in active distribution networks: A comprehensive review. *CSEE Journal of Power and Energy Systems,* 8(5), 1302-1317. https://doi.org/10.17775/CSEEJPES.2021.05820

Zou, Y., Xu, Y., and Li, J. (2024). Aggregator-network coordinated peer-to-peer multi-energy trading via adaptive robust stochastic optimization. *IEEE Transactions on Power Systems,* 39(6), 7124-7137. https://doi.org/10.1109/TPWRS.2024.3367890

Xingyou Zhang currently works as a Senior Engineer at the Power System Research Center of the State Grid Shandong Electric Power Research Institute. His research includes the power spot mark and power system operation.

Yuanlong Liu currently serves as a Director at the Power Dispatching and Control Center of the State Grid Shandong Electric Power Company. His research focuses on the power spot mark and the power system operation.

Qiang Ma currently works as a Senior Engineer at the Power Dispatching and Control Center of State Grid Shandong Electric Power Company. His research interests are in power spot mark and power system operation.

Shan Li currently works as an Engineer at the Power Dispatching and Control Center of State Grid Shandong Electric Power Company. Her research focuses on the power spot mark.

Congcong Liu currently works as an Engineer at the Power System Research Center of the State Grid Shandong Electric Power Research Institute. Her research focuses on the power spot mark and the virtual power plant.

Jing Yao currently works as an Engineer at the Innovation Center of Beijing TsIntergy Technology Co., Ltd. His research interests include power spot mark and power system operation.